Available online at www.sciencedirect.com
SCIENCE DIRECT®
PERGAMON
International Journal of Heat and Mass Transfer 46 (2003) 3083–3095
International Journal of HEAT and MASS TRANSFER
www.elsevier.com/locate/ijhmt

Computational efficiency improvements of the radiative transfer problems with or without conduction—a comparison of the collapsed dimension method and the discrete transfer method

Subhash C. Mishra *,[1], Prabal Talukdar, D. Trimis, Franz Durst

Institute of Fluid Mechanics (LSTM), University of Erlangen-Nuremberg, Cauerstrasse 4, D-91058 Erlangen, Germany

Received 6 September 2002; received in revised form 22 November 2002

Abstract

This paper deals with the performance evaluation of the collapsed dimension method (CDM) and the discrete transfer method (DTM) in terms of computational time and their abilities to provide accurate results in solving radiation and/or conduction mode problems in a 2-D rectangular enclosure containing an absorbing, emitting and scattering medium. For some pure radiation cases, studies were made for two representative benchmark problems dealing with radiative equilibrium and non-radiative equilibrium. For the combined mode, the transient conduction and radiation problem was solved. The alternating direction implicit scheme was used for the solution of the finite difference part of the energy equation. For the three types of problems considered, tests were performed for a wide range of aspect ratio, extinction coefficient, scattering albedo, conduction–radiation parameter and boundary emissivity. For pure radiation problems, results from the two methods were validated against the results from the Monte Carlo method. For the combined mode, some steady-state results were compared with results available in the literature. For the transient situations, results from the two methods were validated against each other. While both the methods were found to give the same results, the CDM was found to be much more economical than the DTM.

Keywords: Conduction; Heat transfer; Radiation

1. Introduction

Efficiency improvements in most industrial thermal processes are achieved by increased process temperatures. The optimum design of such processes is leading to temperature loads near the existing material limits. In recent years, high-temperature-resistant materials, made not only of ceramics but also of special alloys, have become available to realize high-temperature furnaces, gas turbine combustion chambers and blades, heat exchangers, porous volumetric solar receivers, surface and porous IR-radiant burners, etc. [1]. Experimental and numerical investigations are necessary in order to perform an optimum design and to elucidate the advantages of the temperature increase of such improved processes utilizing advanced high-temperature materials. Numerical computations of flow with heat and mass transfer in such high-temperature appliances require a through consideration of radiative heat transfer. Numerical computations of radiation based on conventional methods such as the zonal method, the Monte Carlo method (MCM), etc., coupled with the finite volume solvers of the conservation equations prove to be laborious

* Corresponding author. Tel.: +49-9131-85-28777; fax: +49-9131-85-29503.
E-mail address: scm_iitg@yahoo.com (S.C. Mishra).
[1] On leave from Department of Mechanical Engineering, Indian Institute of Technology, Guwahati 781039, India.

0017-9310/03/$ - see front matter
doi:10.1016/S0017-9310(03)00075-9

Nomenclature

a_1	anisotropy factor
C_p	specific heat at constant pressure
G	incident radiant energy in discrete transfer method (DTM) formulation
G'	effective incident radiant energy in collapsed dimension method (CDM) formulation
I	effective intensity in CDM formulation
i	intensity in DTM formulation
k	thermal conductivity
L_x	length of the enclosure in the x-direction
L_y	length of the enclosure in the y-direction
M	total number of rays/intensities
N	conduction–radiation parameter
q	heat flux
S	source function
T	dimensional temperature
t	dimensional time

Greek symbols

β	extinction coefficient
θ	non-dimensional temperature
η	collapsing coefficient appearing in CDM formulation
τ	optical thickness/depth
α	planar angle appearing in CDM
Ψ	non-dimensional heat flux
ω	scattering albedo
ξ	non-dimensional time $= k\beta^2 t/\rho C_p$
ρ	density
σ	Stefan–Boltzmann constant
γ	polar angle in DTM
δ	azimuthal angle in DTM
ϵ	emissivity

Subscripts

b	boundary
E	east
L	length
N	north
n	nth ray
R	radiative
S	south
W	west

Superscript

$*$	non-dimensional quantities

and very time consuming. For this reason, numerous investigations [2–4] are currently being carried out worldwide to assess computationally efficient methods. This paper deals with the evaluation of such methods and shows that the CDM provides advantages that should be utilized in treating radiative transport problems with or without heat conduction.

Numerical simulations of the high-temperature appliances mentioned above require multi-dimensional analysis. Treatment of radiative transport in the multi-dimensional geometry is difficult mainly because of the three extra independent variables namely the polar angle, the azimuthal angle and the wavelength. Since there is no way out to get rid of the physical dimensions of the geometry and the wavelength of radiation, all numerical models, except the zonal method and the MCM, deal with different types of discretization schemes to make radiation less and less dependent on angular dimensions. The various methods differ primarily in the angular discretization schemes and the use of either the differential form or the integral form of the radiative transfer equation.

The main objective behind the development of any method for the solution of radiative transport problems, apart from its versatility for various geometries, complex medium conditions, etc., is that the method should be computationally efficient.

The DTM is a widely used method. Because of its successful applications to a wide range of problems [2,3,5–10], it is part of commercial CFD solvers such as FLUENT and CFX.

DTM is a ray tracing method. It employs discretization of the entire spherical solid angle (4π) into a finite number of sub-solid angles. In each sub-solid angle, it assumes radiation to be isotropic. In planar geometry, and in multi-dimensional geometry with an absorbing–emitting medium, it is computationally not very expensive. However, in multi-dimensional geometry with an absorbing, emitting and scattering medium, it requires a large number of rays, and thus becomes computationally expensive. Further, this computational time becomes a great concern especially when one applies this method to combined radiation, conduction and/or convection mode problems, where large numbers of iterations are required for the converged solution. Hence the use of an alternative method having the potential to provide accurate results with better economy is very desirable.

In terms of problem formulation, accuracy of results and computational efforts, the CDM is a promising method [11–15]. Unlike other methods, in this method radiative information from 3-D space is collapsed to a 2-D plane in terms of the effective intensity and the collapsing coefficient. Since in the CDM radiation is viewed in the 2-D plane, all 2-D angular integrations over the polar angle and the azimuthal angle in other methods such as the DTM are replaced with 1-D integrations over the planar angle. This collapsing of angular dimension

brings many simplifications and makes this method computationally very efficient. This method has been successfully applied to a large class of problems dealing with pure radiation [11,13,15] and also conjugate conduction and radiation [12,14].

Although the accuracy aspect of the CDM has been well established in earlier studies, with reference to a competitive method such as the DTM or any other methods, its economy aspect has so far not been investigated. This is very important when one has to choose for a method among more than 12 methods that are available.

The DTM possesses features of the flux method, the zonal method and the MCM, and is therefore a method of choice over many other methods. As both the CDM and the DTM are ray tracing methods, for comparison of the economy aspect of the CDM, the DTM is suitable as the reference method.

In this work, both the CDM and DTM are used first to solve two benchmark radiative transport problems in a 2-D rectangular enclosure in which only radiative information is required. The first benchmark problem belongs to radiative equilibrium, while the other belongs to non-radiative equilibrium. For these two problems, for a range of parameters such as the extinction coefficient, the scattering albedo and the aspect ratio, the CDM and the DTM results are compared and CPU times are discussed. Next, transient conduction and radiation heat transfer in a 2-D gray enclosure is considered. This is relatively a complex problem, as for the chosen 2-D rectangular geometry, very few studies [16,17] are available, and they deal with steady-state situations. For the transient case, some results for a black enclosure have been presented in [18]. In all these studies [16–18], the applicability of different methods for multi-dimensional conduction–radiation problems was tested. The objective behind choosing the third problem, therefore, is also to check the applicability of the CDM and the DTM for this problem, and thereby to see how the results from the two methods match at different time levels, and compared with the DTM, how much less time the CDM takes. This comparison is made for various values of aspect ratio, conduction–radiation parameter, scattering albedo, extinction coefficient and hot boundary emissivity. Further, as part of the validation of the combined mode results from the two methods, for some cases, the results are compared with those available in the literature [14,16,18].

2. Formulation

The 2-D rectangular geometry under consideration is shown in Fig. 1. All four boundaries are diffuse and gray, and the contained homogeneous medium is absorbing, emitting and scattering. Thermophysical properties such as density ρ, specific heat C_p, thermal conductivity k and the optical property, extinction coefficient β, are assumed to be constant. For the three types of problems considered in this work, specifications are as follows.

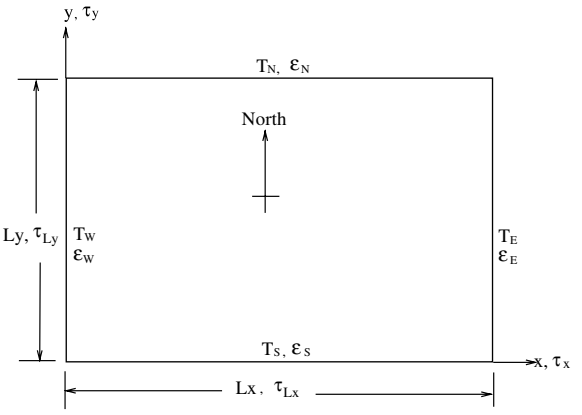

Fig. 1. Geometry and the coordinates of the problem under consideration.

Problem 1. The south boundary of the 2-D enclosure is at some finite temperature T_S and is thus the radiation source. The other three boundaries are cold (at zero temperature). The temperature of the medium is unknown. This case is the representative of a 2-D benchmark radiative equilibrium problem.

Problem 2. All four boundaries of the enclosure are cold and the temperature of the medium is uniform and constant. The absorbing, emitting and scattering medium is thus the known radiation source. This case is the representative 2-D benchmark problem for the validation of any method for solving only the radiative part of a non-radiative equilibrium problem.

Problem 3. Initially at time $t = 0$, the entire system is at some finite temperature T_0. For time $t > 0$, the south boundary is brought to temperature $T_S = 2T_0$. The temperature of the stationary conducting–radiating participating medium is unknown. This is a combined mode problem. It belongs to the class of non-radiative equilibrium problems in which both conduction and radiation modes have to be solved together.

Of the three problems chosen above, Problem 3 is the general one. Hence the formulation is given for that case. Problems 1 and 2 are special cases of Problem 3.

In the absence of convection and heat generation, for a 2-D rectangular geometry, the equation for conservation of total energy is

$$\rho C_p \frac{\partial T}{\partial t} = \frac{\partial}{\partial x}\left(k\frac{\partial T}{\partial x}\right) + \frac{\partial}{\partial y}\left(k\frac{\partial T}{\partial y}\right) - \nabla \cdot q_R \quad (1)$$

For constant thermal conductivity k, in non-dimensional form, Eq. (1) is written as

$$\frac{\partial \theta}{\partial \xi} = \frac{\partial^2 \theta}{\partial \tau_x^2} + \frac{\partial^2 \theta}{\partial \tau_y^2} - \frac{1}{4N}\nabla \cdot \Psi_R \quad (2)$$

where $\tau_x = \beta x$ and $\tau_y = \beta y$ are the optical coordinates in the x and y coordinate directions (Fig. 1), respectively. It should be noted that in Eq. (1), $\nabla = (\partial/\partial x + \partial/\partial y)$ and in Eq. (2), $\nabla = (\partial/\partial \tau_x + \partial/\partial \tau_y)$. With T_{ref} as the reference temperature, in Eq. (2), in non-dimensional form, the temperature θ, the conduction–radiation parameter N, the radiative heat flux Ψ_R and the time ξ are defined as

$$\theta = \frac{T}{T_{ref}}, \quad N = \frac{k\beta}{4\sigma T_{ref}^3}, \quad \Psi_R = \frac{q_R}{\sigma T_{ref}^4}, \quad \xi = \frac{t}{\frac{\rho C_p}{k\beta^2}} = \frac{k\beta^2 t}{\rho C_p}$$

For Problem 3, the initial and boundary conditions are as follows:

$$\begin{array}{ll} \text{Initial condition:} & \theta(\tau_x, \tau_y, 0) = 0.5 \\ \text{Boundary conditions:} & \theta(0, \tau_y, \xi) = 0.5 \\ & \theta(\tau_{L_x}, \tau_y, \xi) = 0.5 \\ & \theta(\tau_x, 0, \xi) = 1.0 \\ & \theta(\tau_x, \tau_{L_y}, \xi) = 0.5 \end{array} \quad (3)$$

For solving Eq. (2) by any of the numerical techniques such as the finite difference method, the finite element method, the finite volume method, etc., information about the divergence of the radiative heat flux $\nabla \cdot \Psi_R$ is required first. Unlike other methods, including the DTM considered here, since CDM views radiation differently, the expressions for $\nabla \cdot \Psi_R$ and the other associated quantities such as incident radiation, intensity, etc., are different in the CDM and the DTM. Therefore, formulations for the evaluation of $\nabla \cdot \Psi_R$ in the two methods are presented briefly below. More details on the use of the two methods, in the context of the present paper, can be found in papers by Mishra and co-workers [11–15].

2.1. Collapsed dimension method formulation

In the CDM, divergence of radiative heat flux $\nabla \cdot \Psi_R$ is given by

$$\nabla \cdot \Psi_R = \eta(1-\omega)\left(\pi\theta^4 - \frac{G'^*}{2}\right) \quad (4)$$

where η is the collapsing coefficient, ω is the scattering albedo and G'^* is the non-dimensional effective incident radiation. In the CDM, G'^* is given by

$$G'^* = \frac{G'}{\frac{\sigma T_{ref}^4}{2}} = \int_0^{2\pi} I^*(\alpha)\,d\alpha \quad (5)$$

where I^* $(= I/(\sigma T_{ref}^4/2))$ is the non-dimensional effective intensity and α is the angle of the effective intensity measured from the control surface. It should be noted that in the CDM, collapsing of the 3-D radiative information to the 2-D solution plane in terms of the effective intensity I^* is made feasible by the collapsing coefficient η. More details on this can be found in [11,13].

In Eq. (5), the effective intensity I^* at any optical depth τ in direction α in the solution plane is found from the recursive use of the following equation:

$$I^*_{n+1} = I^*_n \exp(-\tau\eta) + S'^*[1 - \exp(-\tau\eta)] \quad (6)$$

In any ray tracing method such as the CDM, the DTM, etc., a recursive relation (like Eq. (6)) is obtained directly from the integral form of the radiative transfer equation by performing integrations over a small optical path-leg τ such that the source function S'^* can be assumed to be constant and hence it can be taken outside the integral. Therefore, in the above equation, the optical path-leg τ between the downstream point $(n+1)$ and the upstream point n is small enough and the source function S'^* given by Eq. (7) is constant over the optical path-leg τ.

In the 2-D problems considered here, the constant value of the source function S'^* is taken as its value at the exact middle of the optical path-leg. This value of the source function at the middle of the optical path-leg is computed using the bilinear interpolation of the source functions at the four corners of the control volume to which the effective intensity belongs. Source functions at the corner points of the control volumes are known from the previous iteration. In the first iteration, computations start with some guess values.

If anisotropy of the medium is approximated by linear anisotropic phase function $(p(\alpha' \to \alpha) = 1 + a_1 \sin\alpha \times \sin\alpha')$, the source function S'^* in terms of G'^* and Ψ_R is given by

$$S'^* = (1-\omega)\theta^4 + \frac{\omega}{2\pi}(G'^* + 2a_1 \sin\alpha \Psi_R) \quad (7)$$

where a_1 is the anisotropy factor and Ψ_R is the non-dimensional net radiative heat flux. In the CDM, Ψ_R is given by

$$\Psi_R = \frac{1}{2}\left[\int_{\alpha=0}^{\pi} I^*(\alpha)\sin\alpha\,d\alpha - \int_{\alpha=\pi}^{2\pi} I^*(\alpha)\sin\alpha\,d\alpha\right] \quad (8)$$

In the CDM, intensities are always traced from the boundaries. If in Eq. (6), for the given direction α, if the upstream point n lies on the boundary, then $I^*_n = I^*_0$, and its values have to be found using the radiative boundary condition. For a diffuse–gray boundary with temperature T_b and emissivity ϵ_b, the boundary effective intensity in the CDM is given by

$$I^*_0 = \frac{\epsilon_b T_b^4}{T_{ref}^4} + \frac{1-\epsilon_b}{2}\int_{\alpha=0}^{\pi} I^* \sin\alpha\,d\alpha \quad (9)$$

where the first and the second terms on the right-hand side represent the emitted and reflected components of the boundary effective intensity, respectively.

For the evaluation of G'^* and Ψ_R, Eqs. (5) and (8) are numerically integrated as

$$G'^* = \int_0^{2\pi} I^*(\alpha)\,\mathrm{d}\alpha \approx \sum_{n=1}^{M} I^*(\alpha_n)\,\Delta\alpha_n \tag{10}$$

$$\Psi_R = \frac{1}{2}\left[\int_0^{\pi} I^*(\alpha)\sin\alpha\,\mathrm{d}\alpha - \int_{\pi}^{2\pi} I^*(\alpha)\sin\alpha\,\mathrm{d}\alpha\right] \approx \frac{1}{2}\left[\sum_{n=1}^{M/2} c_n I^*(\alpha_n) - \sum_{n=M/2}^{M} c_n I^*(\alpha_n)\right] \tag{11}$$

where the weight factor is

$$c_n = \left|\cos\left(\alpha_n + \frac{\Delta\alpha_n}{2}\right) - \cos\left(\alpha_n - \frac{\Delta\alpha_n}{2}\right)\right| \tag{12}$$

In Eqs. (10) and (11), M is the number of effective intensities spanned over $0 \leq \alpha \leqslant 2\pi$, and in Eq. (12), $\Delta\alpha_n$ is the discrete angle in the 2-D plane over which the nth effective intensity is assumed to be isotropic. In the present case, $\Delta\alpha_n$ is the same for all effective intensities.

To solve the energy equation (Eq. (2)), $\nabla\cdot\Psi_R$ given by Eq. (4) is substituted in Eq. (2). This yields the desired governing integro-differential equation to be solved in the CDM:

$$\frac{\partial\theta}{\partial\xi} = \frac{\partial^2\theta}{\partial\tau_x^2} + \frac{\partial^2\theta}{\partial\tau_y^2} - \frac{1}{4N}\eta(1-\omega)\left(\pi\theta^4 - \frac{G'^*}{2}\right) \tag{13}$$

For Problem 1, which is representative of the radiative equilibrium case, $\nabla\cdot\Psi_R = 0$, meaning that only the radiation mode is present. As a result, in this case, the source function (Eq. (7)) is simplified. This simplified form of the source function is the one which results from the substitution of $\omega = 1$. Further, in this case, the temperature θ of the medium is unknown. Once G'^* has been calculated, θ is found from

$$\theta = \left(\frac{G'^*}{2\pi}\right)^{1/4} \tag{14}$$

For Problem 2, $\nabla\cdot\Psi_R \neq 0$. Here the temperature θ of the medium is known and Eq. (7) is the required source function. For all three types of problems considered, radiative heat flux is computed using Eq. (11). The collapsing coefficient η values for any β and ω are computed from the expressions given in [11].

2.2. Discrete transfer method formulation

Except for the CDM, in all other methods, including the DTM, the divergence of the radiative heat flux $\nabla\cdot\Psi_R$ appearing in Eq. (2) is given by

$$\nabla\cdot\Psi_R = 4(1-\omega)\left(\theta^4 - \frac{G^*}{4\pi}\right) \tag{15}$$

where G^* is the non-dimensional incident radiation. It is given by, and in the DTM it is numerically computed from,

$$G^* = \frac{G}{\dfrac{\sigma T_{ref}^4}{\pi}} = \int_{\delta=0}^{2\pi}\int_{\gamma=0}^{\pi} i^*(\gamma,\delta)\sin\gamma\,\mathrm{d}\gamma\,\mathrm{d}\delta \approx \sum_{k=1}^{M_\delta}\sum_{l=1}^{M_\gamma} i^*(\gamma_k,\delta_l)\sin\gamma_k\sin(\Delta\gamma)\,\Delta\delta \tag{16}$$

where i^* $(= i/(\sigma T_{ref}^4/\pi))$ is the non-dimensional intensity, γ is the polar angle, δ is the azimuthal angle, and M_γ and M_δ are the number of intensities i^* considered over the complete span of γ $(0 \leqslant \gamma \leqslant \pi)$ and δ $(0 \leqslant \delta \leqslant 2\pi)$, respectively.

With similar arguments to those given for the CDM, in the DTM the recursive relation for finding the intensity i^* at any downstream point $(n+1)$ in the ray direction (γ,δ) is given by

$$i^*_{n+1} = i^*_n\exp(-\tau) + S^*[1-\exp(-\tau)] \tag{17}$$

The boundary intensity i^*_0 in the DTM is given by

$$i^*_0 = \frac{\epsilon_b T_b^4}{T_{ref}^4} + \frac{(1-\epsilon_b)}{\pi}\int_{\delta=0}^{2\pi}\int_{\gamma=0}^{\pi/2} i^*(\gamma,\delta)\cos\gamma\sin\gamma\,\mathrm{d}\gamma\,\mathrm{d}\delta \tag{18}$$

For the linear anisotropic phase function $(p((\gamma',\delta')\to(\gamma,\delta)) = 1 + a_1\cos\gamma\cos\gamma')$, the source function appearing in Eq. (17), in terms of G^* and Ψ_R is given by

$$S^* = (1-\omega)\theta^4 + \frac{\omega}{4\pi}[G^* + a_1\pi\cos\gamma\,\Psi_R(\tau)] \tag{19}$$

It should be noted that as for the CDM, in the DTM also, in this work the constant value of the source function at the exact middle of the optical path-leg τ was computed using the bilinear interpolation of the source functions at the four corner points of the control volume.

In the DTM, the net radiative heat flux Ψ_R is given by and numerically computed from,

$$\Psi_R = \frac{1}{\pi}\int_{\delta=0}^{2\pi}\int_{\gamma=0}^{\pi} i^*(\gamma,\delta)\sin\gamma\cos\gamma\,\mathrm{d}\gamma\,\mathrm{d}\delta \approx \frac{1}{\pi}\sum_{k=1}^{M_\delta}\sum_{l=1}^{M_\gamma} i^*(\gamma_k,\delta_l)\cos\gamma_k\sin\gamma_k\sin(\Delta\gamma)\,\Delta\delta \tag{20}$$

To solve energy Eq. (2), the divergence of radiative heat flux given by Eq. (15) is substituted in Eq. (2), which yields the desired governing integro-differential equation to be solved in the DTM.

$$\frac{\partial\theta}{\partial\xi}=\frac{\partial^2\theta}{\partial\tau_x^2}+\frac{\partial^2\theta}{\partial\tau_y^2}-\frac{1-\omega}{N}\left(\theta^4-\frac{G^*}{4\pi}\right) \tag{21}$$

For solving Problem 1 using the DTM, the source function is the one which results from substitution of $\omega=1$ in Eq. (19). The unknown temperature θ of the medium is obtained from Eq. (15) by setting $\nabla\cdot\Psi_R=0$:

$$\theta=\left(\frac{G^*}{4\pi}\right)^{1/4} \tag{22}$$

Eq. (20) for the radiative heat flux is applicable to all types of problems.

3. Results and discussion

Here the CDM and DTM results for the three types of problems are presented. All results from the two methods are for grid and ray independent situations. Although numbers of rays required in the two methods are different, for a particular situation the grid size in the two methods was kept the same.

For Problems 1 and 2, for aspect ratio $L_x/L_y=1$, the CDM and the DTM results were compared against the MCM results generated by the authors. For Problem 3, results from the two methods were validated against each other. The computational times required in the CDM and the DTM are presented for various conditions.

In Problem 1, the CDM and the DTM results for heat flux variations along the hot (south) boundary and the centreline ($x/L_x=0.5$) emissive power distributions were compared for different values of the extinction coefficient β and aspect ratio L_x/L_y. In Problem 2, results from the two methods were compared for the effects of β, scattering albedo ω and L_x/L_y. For the combined mode problem (Problem 3), first the CDM and the DTM results for the steady-state temperature θ obtained from the 2-D rectangular geometry codes for $L_x/L_y=10.0$ were validated by comparison with the 1-D CDM results [14]. For $L_x/L_y=1.0$, for some cases, steady-state results from the two methods were compared with the numerical data presented in the literature [16,18]. Next, to assess the performance of the two methods for the transient situation, the CDM and the DTM results at different instants ξ were compared against each other over a wide range of values of conduction–radiation parameter N, extinction coefficient β, scattering albedo ω, hot boundary emissivity ϵ_S and L_x/L_y. Transient problems in both methods were solved with the time step $\Delta\xi=0.001$, and steady-state conditions were assumed to have been achieved when the temperature difference between the two consecutive time levels at each grid point did not exceed 0.00001. It should be noted that in all cases where the effects of aspect ratio L_x/L_y were studied, L_y was always kept at unity. All computations were performed on a SUN Ultra-60 workstation (2× CPU UltraSPARC 360 MHz, RAM 1280 MB at 120 MHz).

In all results presented below, the temperature of the south boundary T_S is the reference temperature T_{ref} for Problems 1 and 3. The medium temperature T_g is the T_{ref} for Problem 2.

3.1. Problem 1: Radiative equilibrium—boundary emission case

In Figs. 2 and 3, the CDM and the DTM results are compared for non-dimensional heat flux Ψ_R and emissive power $(T/T_S)^4$ distributions. For these results, all boundaries are black and the medium is absorbing, emitting and isotropically scattering. The south boundary is hot, whereas the other three boundaries are cold. For grid and ray independent situations, in the CDM, the results presented in Figs. 2 and 3 required 20×20 control volumes and 64 rays. However, in the DTM, for extinction coefficients $\beta=0.1$, 1.0 and 2.0, 12×24 rays were used, and for $\beta=3.0$ and 5.0, 24×48 rays were used.

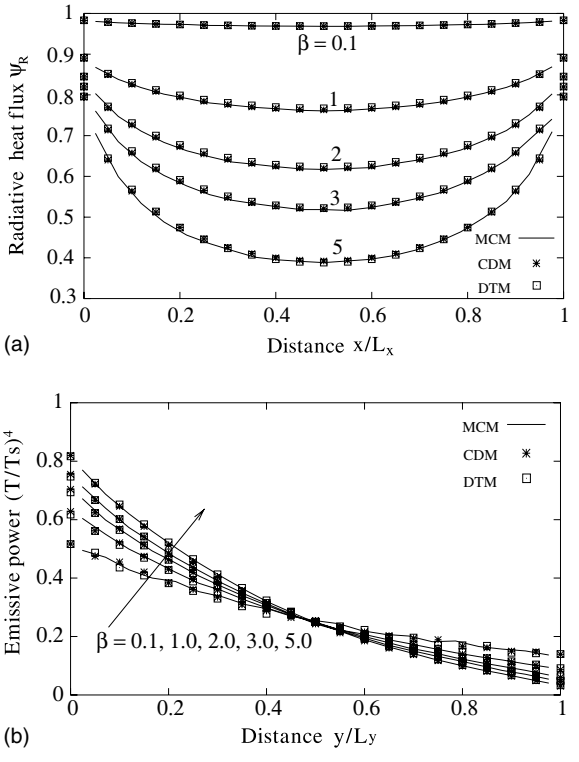

Fig. 2. Comparison of the CDM and the DTM results with the MCM results for the effects of extinction coefficient β on (a) heat flux Ψ_R along the hot (south) boundary and (b) the centreline emissive power $(T/T_S)^4$.

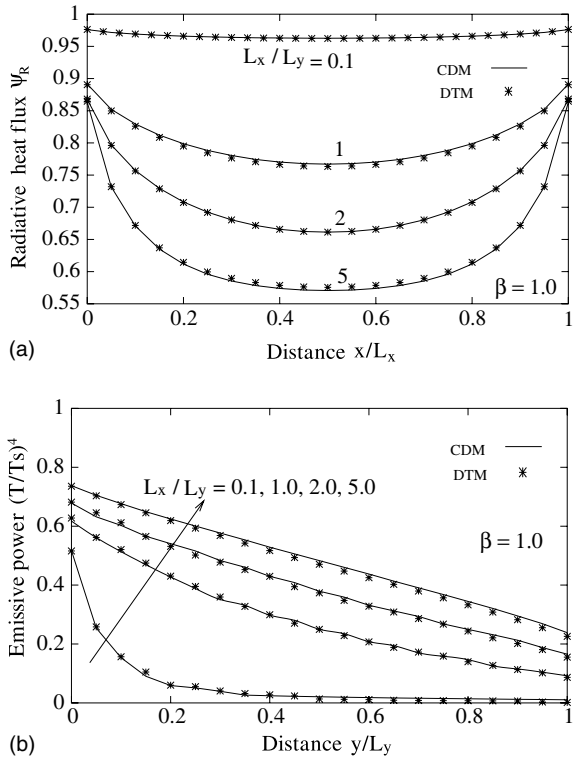

Fig. 3. Comparison of the CDM and the DTM results for the effects of aspect ratio L_x/L_y on (a) heat flux Ψ_R along the hot (south) boundary and (b) the centreline emissive power $(T/T_S)^4$.

In Fig. 2(a), the CDM and the DTM results for the variations of Ψ_R along the hot (south) boundary are compared for various values of the extinction coefficient β. In Fig. 2(b), comparisons of emissive power $(T/T_S)^4$ variations at $x/L_x = 0.5$ along y/L_y are made. It can be seen that both the CDM and DTM results compare well with the MCM results. For the level of accuracy shown in Fig. 2, for $\beta = 0.1$, 1.0, 2.0, 3.0 and 5.0, CPU times in the CDM were 9.65, 24.23, 39.74, 61.36 and 109.28 s, respectively, and the corresponding CPU times for the DTM were 31.21, 138.83, 229.95, 1399.78 and 2501.48 s, respectively. Thus, from above results it is seen that for the same level of accuracy, the CDM is much more faster than the DTM.

In Fig. 3(a) and (b), for $\beta = 1.0$, the CDM and DTM results for Ψ_R and $(T/T_S)^4$ are compared against each other for $L_x/L_y = 0.1$, 1.0, 3.0 and 5.0. For all values of the aspect ratio L_x/L_y, the CDM results compare very well with the DTM results. In this case, for $L_x/L_y = 0.1$, 1.0, 2.0, and 5.0, the CPU times in the CDM were 9.56, 24.23, 28.92, and 29.76 s, respectively, and the corresponding CPU times in the DTM were 55.49, 138.83, 162.17, and 181.51 s, respectively.

3.2. Problem 2: Non-radiative equilibrium—isothermal medium emission case

In this case, all four boundaries are black and cold. The absorbing, emitting and isotropically scattering medium is at constant temperature. In Fig. 4(a)–(c), variations of non-dimensional radiative heat flux Ψ_R along the south boundary are compared. In this case, in the CDM 64 rays were used, while in the DTM, 12×24 rays were used for $\beta = 0.1$ and 1.0 and 24×48 rays were

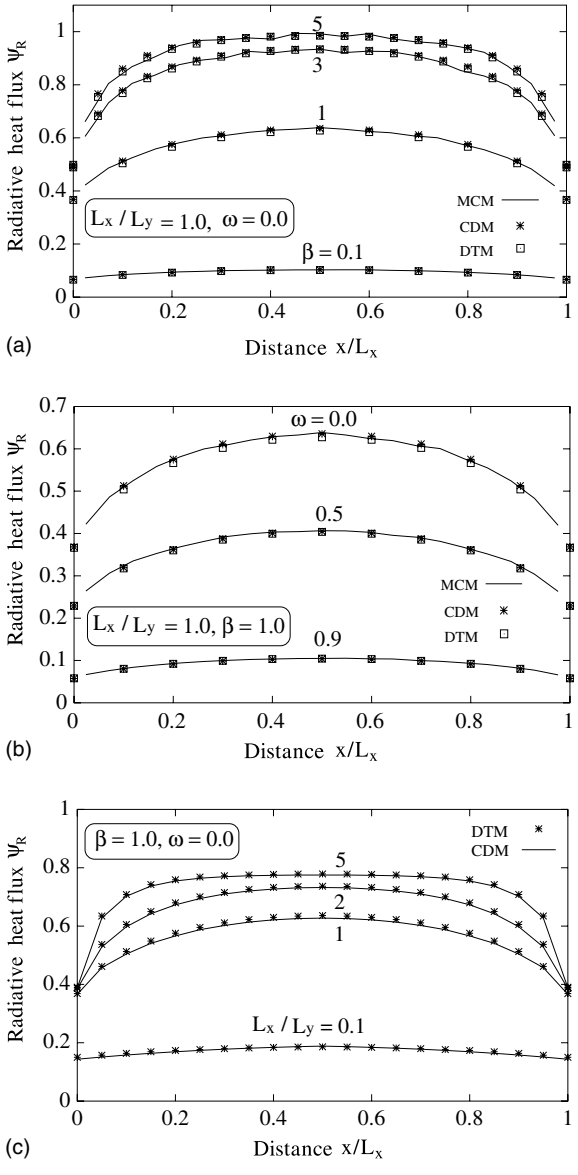

Fig. 4. Comparison of the CDM and the DTM results for heat flux Ψ_R variations along the south boundary for the effects of (a) extinction coefficient β, (b) scattering albedo ω and (c) aspect ratio L_x/L_y.

used for $\beta = 3.0$ and 5.0. For $L_x/L_y = 1.0$, in Fig. 4(a) and (b), the CDM and the DTM results for different values of β and ω are compared with the MCM results. Both the CDM and DTM are found to give a very good comparison. In Fig. 4(c), for $\beta = 1.0$ and $\omega = 0.0$, results from the two methods are compared for $L_x/L_y = 0.1$, 1.0, 2.0 and 5.0. The CDM results are found to compare very well with the DTM results. For the results presented in Fig. 4(b), for $\omega = 0.5$ and 0.9, CPU times in the CDM are 1.64 and 2.58 s, respectively. The corresponding CPU times in the DTM are 13.57 and 21.91 s. In problem 2, for $\omega = 0.0$, no iterations are required. The CPU times in both the methods are negligible.

It is to be noted that the situations which require iterations, for different sets of parameters, even though the ratio of the number of rays in the CDM and the DTM are the same, the ratio of the CPU times in the two methods are different. This is for the reason that the number of iterations required for the converged solutions are different for different sets of parameters and CPU times per iteration in the two methods are also different. However, for a given set of parameters, the number of iterations in the two methods have been found the same.

3.3. Problem 3: Combined mode—transient conduction and radiation

Having validated the CDM and the DTM against the MCM, and also against each other for Problems 1 and 2 above, before proceeding to the complex situation, it is important to check that for higher aspect ratios, such as $L_x/L_y = 10.0$, results from the two methods for the 2-D rectangular enclosure problem compare satisfactorily with the 1-D planar medium results [14]. Next, as part of the further validation studies, for a square enclosure ($L_x/L_y = 1.0$), for three different values of the conduction–radiation parameter N and the extinction coefficient β, the CDM and the DTM steady-state temperature θ results are compared with the numerical data provided in the literature [16,17]. It should be noted that for grid and ray independent situations, for all results presented in the following paragraphs, in both the methods runs were taken for 20×20 control volumes, and in the CDM 64 rays and in the DTM 24×48 rays were used.

In Fig. 5(a)–(c), for $L_x/L_y = 10.0$, at $x/L_x = 0.5$, the variations in the temperature θ of the medium along y/L_y are given. When L_x/L_y is large ($L_x = 10, L_y = 1$), the effects of the east and west boundaries are insignificant and the centreline temperature in this case approaches that for the temperature distribution for the 1-D planar medium having same boundary conditions at the south and north boundaries [14]. This fact is demonstrated in

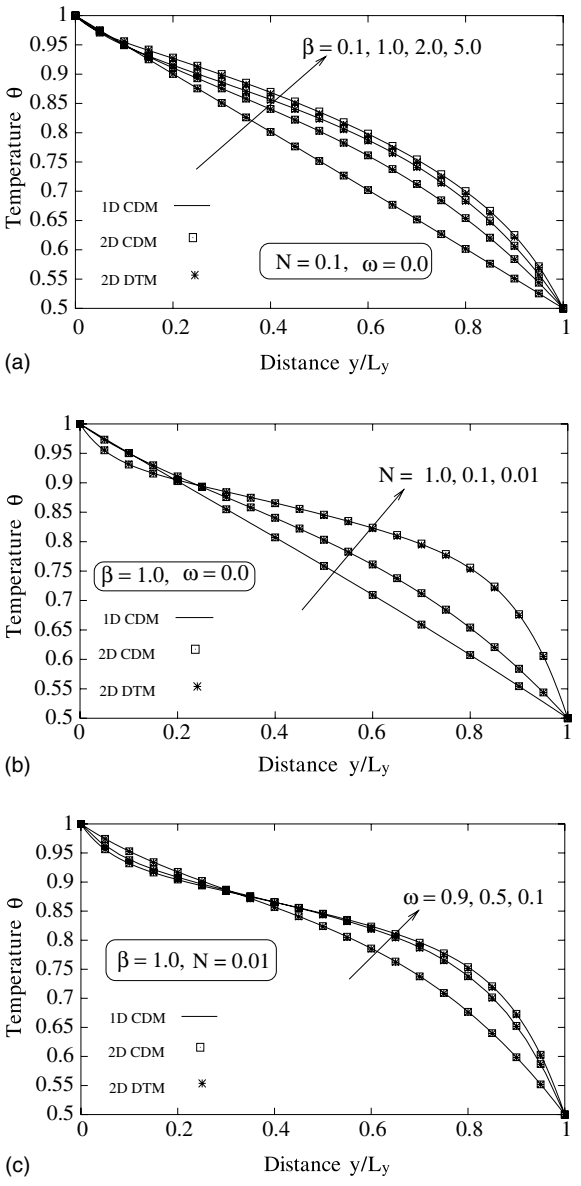

Fig. 5. Comparison of the 2-D CDM and the 2-D DTM results for the steady-state centreline temperature θ distribution for aspect ratio $L_x/L_y = 10$ with 1-D CDM results [14] for the effects of (a) extinction coefficient β, (b) conduction–radiation parameter N and (c) scattering albedo ω.

Fig. 5(a)–(c). For all results presented in Fig. 5, the boundaries are black. It should be noted that in these figures, the 2-D CDM and the 2-D DTM results are the steady-state results for the transient problem.

For scattering albedo $\omega = 0.0$ and the conduction–radiation parameter $N = 0.1$, in Fig. 5(a), θ results from the 2-D CDM and the 2-D DTM codes for extinction coefficient $\beta = 0.1$, 1.0, 2.0 and 5.0, are compared

against the 1-D CDM results. In Fig. 5(b), for $\beta = 1.0$ and $\omega = 0.0$, these comparisons are made for $N = 1.0$, 0.1 and 0.01. For $\beta = 1.0$ and $N = 0.01$, in Fig. 5(c), comparisons are made for $\omega = 0.1$, 0.5 and 0.9. It can be seen that in all cases, when the effects of the side boundaries are negligible, the 2-D CDM and the 2-D DTM results obtained by solving the transient problems match perfectly with the 1-D planar medium results.

In Table 1, for three different values of β (0.1, 1.0 and 5.0) and N (0.01, 0.1 and 1.0), the CDM and DTM temperature results for 20×20 control volumes are compared with those of Yuen and Takara [16] and Wu and Ou [18], which are for 10×10 and 20×20 control volumes, respectively. For the black square enclosure ($L_x/L_y = 1.0$) for all these results, the medium is absorbing–emitting ($\omega = 0.0$). It can be seen from Table 1 that the results from the CDM and the DTM are in very good agreement with each other and also with those in the literature obtained using two different methods.

After having proved the correctness of the 2-D CDM and the 2-D DTM codes above, below the temperature θ distributions at various instants ξ obtained from the CDM and the DTM are compared and remarks about the CPU times of the two methods are made.

In Fig. 6(a)–(c), θ results from the CDM and DTM are compared for $N = 0.01$, 0.1 and 1.0 respectively. All these results are for $L_x/L_y = 1.0$, $\beta = 1.0$ and $\omega = 0.0$. The θ results are compared at time $\xi = 0.001$, 0.005, 0.015, 0.040 and steady state. For all values of N, at all times ξ, the CDM results compare very well with the DTM results. For $N = 0.01$, 0.1 and 1.0, CPU times in the CDM were 144.69, 402.37 and 488.18 s, respectively. The corresponding CPU times in the DTM were 3398.39, 10 139.58 and 10 492.26 s. The CDM is thus more than 20 times faster than the DTM.

From Fig. 6(a)–(c), it is observed that in the early stage ($\xi = 0.001$), N does not have much effect on the θ distribution. However, as time passes, the effect increases. For the radiation-dominated situation ($N = 0.01$, Fig. 6(a)), owing to an increased contribution from radiation, at any instant ξ, the temperature in the medium is high. Further, since radiation is an instantaneous process, when its dominance is greater (for lower values of N), the steady-state is reached fast. As can be seen from Fig. 6(a)–(c), the non-dimensional steady-state times ξ for $N = 0.01$, 0.1 and 1.0 are 0.088, 0.257 and 0.311 respectively.

In Fig. 7(a)–(c), comparisons of the CDM and the DTM results are made for the effects of the extinction coefficient β. For these results, the values of L_x/L_y, ω and N are 1.0, 0.1 and 0.0 respectively. For all cases, the CDM and the DTM results are found to match very well. For $\beta = 0.1$, 1.0 and 5.0, CPU times in the CDM were 77.12, 402.37 and 442.30 s, respectively. For the

Table 1
Comparison of the steady-state centreline ($x/L_x = 0.5$) temperature θ results from the CDM and the DTM at various locations along y/L_y with results in [16,18] for different values of the extinction coefficient β and conduction–radiation parameter N; $L_x/L_y = 1.0$, $\omega = 0.0$, all boundaries are black

β	N	Method	Centreline θ at different y/L_y				
			1.0	0.7	0.5	0.3	0.0
0.1	0.1	Ref. [16]	0.500	0.561	0.626	0.733	1.000
		Ref. [18]	0.500	0.563	0.630	0.733	1.000
		DTM	0.500	0.561	0.626	0.734	1.000
		CDM	0.500	0.561	0.626	0.734	1.000
1.0	1.0	Ref. [16]	0.500	0.564	0.630	0.737	1.000
		Ref. [18]	0.500	0.560	0.630	0.733	1.000
		DTM	0.500	0.564	0.630	0.737	1.000
		CDM	0.500	0.564	0.630	0.737	1.000
1.0	0.1	Ref. [16]	0.500	0.589	0.661	0.763	1.000
		Ref. [18]	0.500	0.590	0.663	0.760	1.000
		DTM	0.500	0.594	0.663	0.760	1.000
		CDM	0.500	0.594	0.663	0.759	1.000
1.0	0.01	Ref. [16]	0.500	0.653	0.726	0.807	1.000
		Ref. [18]	0.500	0.663	0.725	0.791	1.000
		DTM	0.500	0.665	0.725	0.790	1.000
		CDM	0.500	0.666	0.725	0.789	1.000
5.0	0.1	Ref. [16]	0.500	0.585	0.689	0.834	1.000
		Ref. [18]	0.500	0.626	0.707	0.802	1.000
		DTM	0.500	0.628	0.708	0.802	1.000
		CDM	0.500	0.626	0.706	0.802	1.000

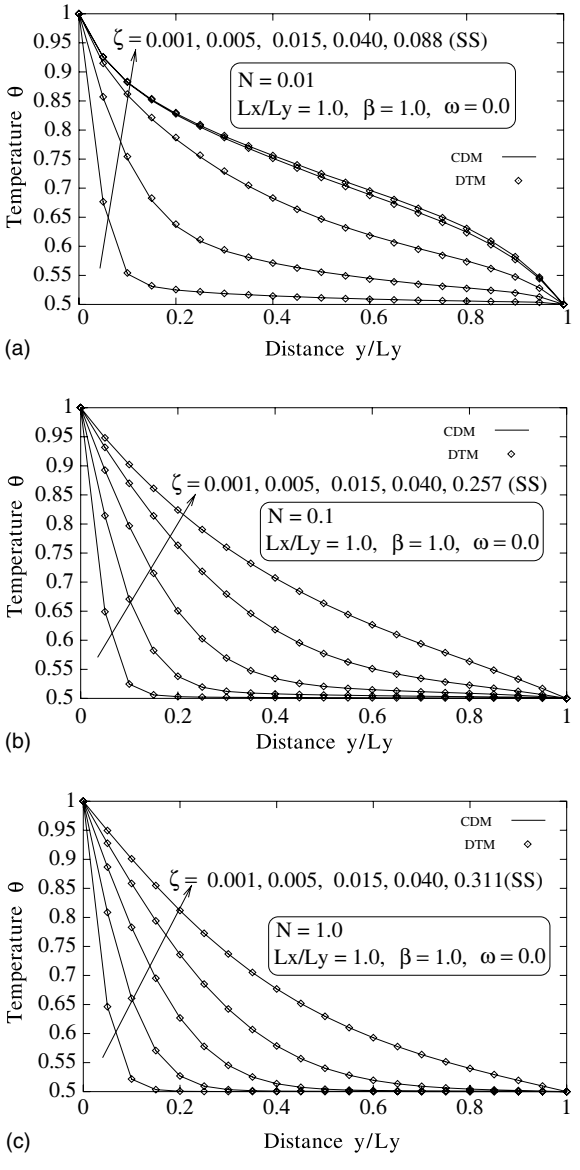

Fig. 6. Comparison of the CDM and the DTM results for the centreline temperature θ distribution at time $\xi = 0.001$, 0.005, 0.015, 0.04 and steady state (SS) for conduction–radiation parameter N (a) 0.01, (b) 0.1 and (c) 1.0.

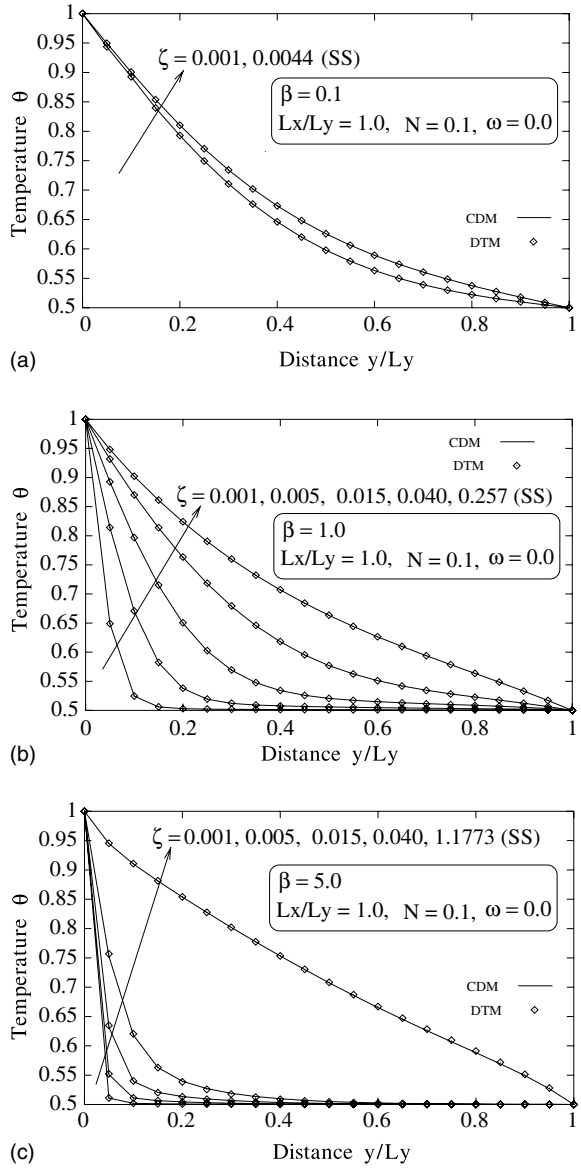

Fig. 7. Comparison of the CDM and the DTM results for the centreline temperature θ distribution at time $\xi = 0.001$, 0.005, 0.015, 0.04 and SS for extinction coefficient β (a) 0.1, (b) 1.0 and (c) 5.0.

DTM, the corresponding CPU times were 1710.11, 10 139.58 and 10 702.83 s. The CDM is more than 22 times faster than the DTM.

From Fig. 7(a)–(c), it is seen that as the medium becomes optically thick, i.e., as β increases, the steady-state is delayed, and the steady-state temperature in the medium increases. However, at any time ξ, the transient temperatures in the medium are lower for higher values of β. With all other parameters fixed, with an increase in β, the increased absorption and scattering in the medium does not allow the radiation from the boundaries to penetrate deep into the medium. As a result of which steady state is delayed.

In Fig. 8(a)–(c), comparisons of the CDM and DTM results are made for the effects of scattering albedo ω. For all these results, θ distributions are presented for $L_x/L_y = 1.0$, $\beta = 1.0$ and $N = 0.01$. It can be seen that as ω increases, the steady-state time increases. This trend is due to the fact that with increase in ω, the medium absorbs and emits less energy and approaches a conduc-

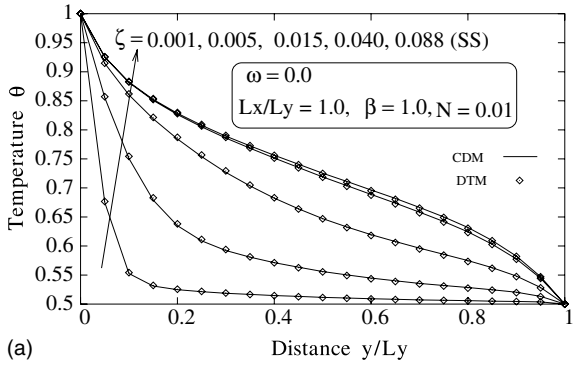

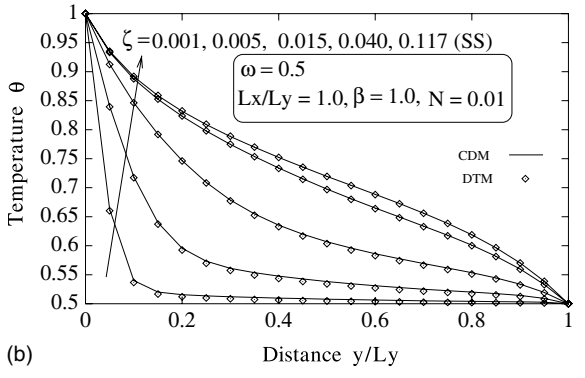

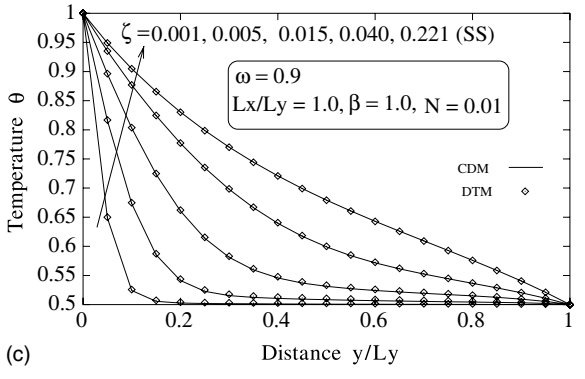

Fig. 8. Comparison of the CDM and the DTM results for the centreline temperature θ distribution at time $\xi = 0.001$, 0.005, 0.015, 0.04 and SS for scattering albedo ω (a) 0.0, (b) 0.5 and (c) 0.9.

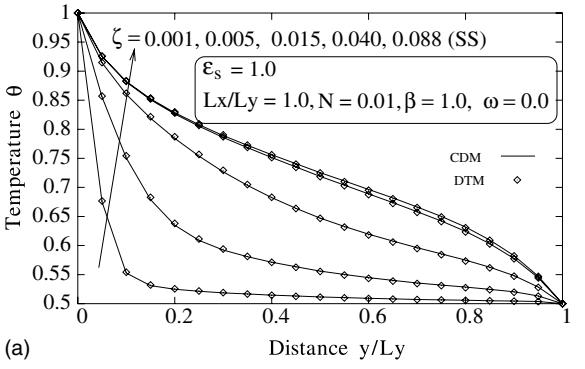

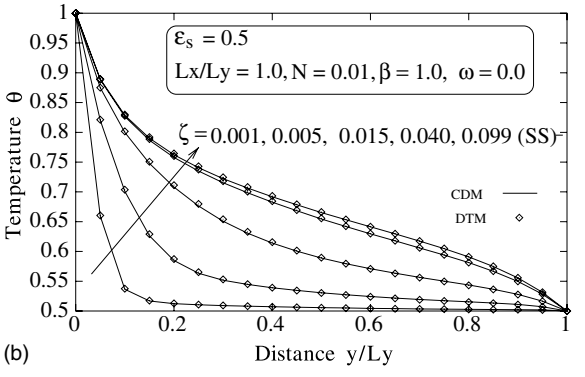

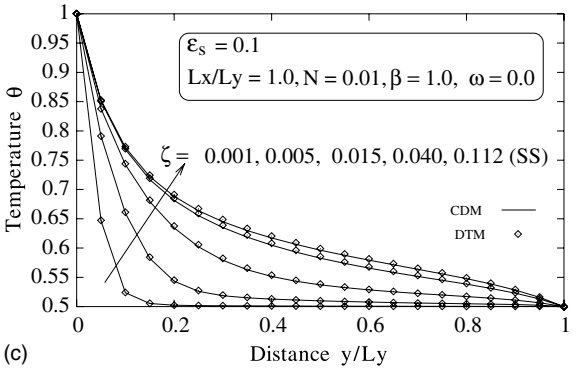

Fig. 9. Comparison of the CDM and the DTM results for the centreline temperature θ distribution at time $\xi = 0.001$, 0.005, 0.015, 0.04 and SS for the hot (south) boundary emissivity ϵ_S (a) 1.0, (b) 0.5 and (c) 0.1.

tion-like situation. For example, for $\omega = 1.0$, $\nabla \cdot \Psi_R = 0.0$, the radiation term does not appear in the energy equation. For all the results presented in Fig. 8, the results from the CDM and the DTM match each other very well. In this case, the CDM is about 22 times faster than the DTM.

Comparisons of the CDM and DTM results for the effects of hot (south) boundary emissivity ϵ_S on θ distributions at different instants ξ are shown in Fig. 9(a)–(c). For these results, the values of β, N, ω and L_x/L_y are 1.0, 0.01, 0.0 and 1.0 respectively. In Fig. 9(a)–(c), the hot (south) boundary emissivity $\epsilon_S = 1.0$, 0.5 and 0.1, respectively. However, for all these results, the other three boundaries, viz. north, east and the west, are black. As in all previous cases, in this case also, it is seen that at all times, the CDM and the DTM results compare with each other very well. The CDM is about 20 times faster than the DTM.

It can be seen from Fig. 9(a)–(c) that when the south boundary is reflecting more ($\epsilon_S = 0.1$), the steady state is

attained late and at any instant ξ, the temperature of the medium is lower. Further, for lower values of ϵ_S, the temperature gradients near the hot boundary are higher. As the hot boundary becomes more reflecting, radiation emanating from the hot boundary becomes weak (see Eq. (9) or (18)), as a result of which sharp gradients are observed near the hot boundary, the temperature at any instant in the medium is lower and, since the radiative contribution decreases, the steady state is reached late.

4. Conclusions, final remarks and outlook

The performance of the CDM and the DTM in terms of the computational time and their abilities to provide accurate results was evaluated for three types of problems. For the boundary emission and the isothermal medium emission cases, the CDM and DTM results for aspect ratio $L_x/L_y = 1$ were compared with the MCM results. For $L_x/L_y \neq 1$, results from the two methods were compared against each other. For the combined mode problem, for the steady state, for the effects of the extinction coefficient β, the conduction–radiation parameter N, and the scattering albedo ω, the 2-D CDM and the 2-D DTM codes for $L_x/L_y = 10.0$ were found to give the same results as given by the CDM code for the 1-D planar medium [14]. For the black square enclosure ($L_x/L_y = 1$), for various values of N and β, the CDM and DTM steady-state results were found to give an excellent comparison with the results available in the literature [16,18]. In this way once the 2-D CDM and the 2-D DTM codes had been validated for the boundary emission, the isothermal medium emission and some steady-state benchmark results for the combined mode problems, transient temperature distributions were found and compared for various parameters such as N, β, ω and ϵ_S. For all the parameters considered, CDM results were found to give an excellent comparison with the DTM results. Further, for all cases, the CDM was found much more economical than the DTM.

In this work, the CDM was applied to a geometrically simple 2-D rectangular enclosure. There is no reason, however, to believe that the advantages of this method, demonstrated in this paper, will diminish as the geometry of the 2-D computational domain becomes more complex. Hence owing to the simplicity of the method and its ability to provide accurate results with much better economy, the authors recommend the use of the CDM for radiative transport problems.

Acknowledgement

This work was supported by a Research Fellowship of the Alexander von Humboldt Foundation.

References

[1] O. Pickenacker, K. Pickenacker, K. Wawrzinek, D. Trimis, W.E.C. Pritzkow, C. Muller, P. Goedtke, U. Papenburg, J. Adler, G. Standke, H. Heymer, W. Tauscher, F. Jansen, Innovative ceramic materials for porous-medium burners I–II, Interceram 48 (5) (1999) 326–330 (6) 424–434.

[2] J.C. Henson, W.M.G. Malalasekara, Comparison of the discrete transfer and Monte Carlo methods for radiative heat transfer in three-dimensional nonhomogeneous scattering media, Numer. Heat Transfer, Part A 32 (1997) 19–36.

[3] P.J. Coelho, J.M. Goncalves, M.G. Carvalho, D.N. Trivic, Modelling of radiative heat transfer in enclosures with obstacles, Int. J. Heat Mass Transfer 41 (4–5) (1998) 745–756.

[4] S.H. Kim, K.Y. Huh, Assessment of the finite-volume method and the discrete ordinate method for radiative heat transfer in a three-dimensional rectangular enclosure, Numer. Heat Transfer, Part B 35 (1999) 85–112.

[5] N.G. Shah, New method of computation of radiation heat transfer in combustion chambers, Ph.D. Thesis, Imperial College, University of London, England, 1979.

[6] P. Docherty, M. Fairweather, Prediction of radiative transfer from non-homogeneous combustion products using the discrete transfer method, Combust. Flame 71 (1988) 79–87.

[7] M. da Graca Carvalho, T. Farias, P. Fontes, Multidimensional modeling of radiative heat transfer in scattering media, J. Heat Transfer 115 (1993) 486–489.

[8] N.W. Bressloff, J.B. Moss, P.A. Rubini, Assessment of a differential total absorptivity solution to the radiative transfer equation as applied in the discrete transfer radiation model, Numer. Heat Transfer, Part B 29 (1996) 381–397.

[9] P.S. Cumber, M. Fairweather, H.S. Ledin, Application of wide band radiation models to non-homogeneous combustion systems, Int. J. Heat Mass Transfer 41 (11) (1998) 1573–1584.

[10] H. Xue, J.C. Ho, Y.M. Cheng, Comparison of different combustion models in enclosure fire simulation, Fire Safety J. 36 (2001) 37–54.

[11] S.C. Mishra, A novel computational approach for the solution of radiative heat transfer problems in participating media, Ph.D. Thesis, IIT Kanpur, India, 1997.

[12] P. Talukdar, S.C. Mishra, Transient conduction and radiation heat transfer with heat generation in a participating medium using the collapsed dimension method, Numer. Heat Transfer, Part A 37 (2001) 79–100.

[13] S.C. Mishra, M. Prasad, Radiative heat transfer in absorbing–emitting-scattering gray media inside 1-D cartesian enclosure using the collapsed dimension method, Int. J. Heat Mass Transfer 45 (3) (2002) 697–700.

[14] P. Talukdar, S.C. Mishra, Analysis of conduction–radiation problem in absorbing–emitting and anisotropically scattering media using the collapsed dimension method, Int. J. Heat Mass Transfer 45 (2002) 2159–2168.

[15] P. Mahanta, S.C. Mishra, Collapsed dimension method applied to radiative transfer problems in complex enclosures with participating medium, Numer. Heat Transfer, Part B 42 (4) (2002) 367–388.

[16] W.W. Yuen, E.E. Takara, Analysis of combined conductive–radiative heat transfer in a two-dimensional rectangular enclosure with a gray medium, J. Heat Transfer 110 (1988) 468–474.
[17] T.Y. Kim, S.W. Baek, Analysis of combined conductive and radiative heat transfer in a two-dimensional rectangular enclosure using the discrete ordinate method, Int. J. Heat Mass Transfer 34 (9) (1991) 2265–2273.
[18] C.Y. Wu, N.R. Ou, Transient two-dimensional radiative and conductive heat transfer in a scattering medium, Int. J. Heat Mass Transfer 37 (17) (1994) 2675–2686.